

Diffusiophoretic Fast Swelling of Chemically Responsive Hydrogels

Chinmay Katke^{1,2}, Peter A. Korevaar³, and C. Nadir Kaplan^{1,2,*}

¹*Department of Physics, Virginia Polytechnic Institute and State University, Blacksburg, Virginia 24061, USA*

²*Center for Soft Matter and Biological Physics, Virginia Polytechnic Institute and State University, Blacksburg, Virginia 24061, USA*

³*Institute for Molecules and Materials, Radboud University, 6525 AJ Nijmegen, The Netherlands*

 (Received 8 September 2023; accepted 1 April 2024; published 15 May 2024)

Acid-induced release of stored ions from polyacrylic acid hydrogels (with a free surface fully permeable to the ion and acid) was observed to increase the gel osmotic pressure that leads to rapid swelling faster than the characteristic solvent absorption rate of the gel. The subsequent equilibration of the diffusing ion concentration across the gel surface diminishes the osmotic pressure. Then, the swollen gel contracts, thereby completing one actuation cycle. We develop a continuum poroelastic theory that explains the experiments by introducing a “gel diffusiophoresis” mechanism: Steric repulsion between the gel polymers and released ions can induce a diffusio-osmotic solvent intake counteracted by the diffusiophoretic expansion of the gel network that ceases when the ion gradient vanishes. For applications ranging from drug delivery to soft robotics, engineering the gel diffusiophoresis may enable stimuli-responsive hydrogels with amplified strain rates and power output.

DOI: 10.1103/PhysRevLett.132.208201

The capability of osmosis to convert modest concentration differences into significant pressures underlies biological processes ranging from turgor pressure regulation in walled cells to the urea-water separation in the kidney, which inspired many applications for chemomechanical energy conversion [1–12]. It also governs hydrogel expansion through solvent imbibition, and has enabled stimuli-responsive micron-scale gels for, e.g., soft actuation or synthetic homeostasis [13–23]. Scaling up these gel designs, however, is hindered by the drastic reduction of their strain rate and power output since a gel with the shortest dimension H and permeability k_f typically absorbs the solvent and deforms at a rate $\tau^{-1} \sim k_f/H^2$. Although increasing the pore size (i.e., higher k_f) mitigates this limitation, it reduces the gel polymer density, compromising on its functionalization and in turn the gel responsiveness to external fields [24–26].

One chemically responsive system that deforms faster than τ^{-1} via a tunable transient osmotic imbalance is the polyacrylic acid (PAA) hydrogel [27]. Under neutral or basic pH, the PAA gel can arrest divalent copper ions Cu^{2+} (or calcium ions Ca^{2+} as a biological signal mediator [27–29]) and contract from its equilibrium height H by forming $\text{COO}^- - \text{Cu}^{2+} - \text{COO}^-$ chelates that remain kinetically stable without external Cu^{2+} [Fig. 1(a)] [30]. When HCl is delivered as a second stimulus, the dissolved acid rapidly displaces Cu^{2+} , releasing it to the fluid phase of the gel [Fig. 1(b)]. Although the formation of the carboxyl (COOH) groups (this time in an acidic condition) favors gel contraction [31–33], the gel temporarily swells by $\sim 10\%$ of H over the total copper decomplexation time τ_{total} if $\tau_{\text{total}} < \tau \equiv H^2/D$ (D : poroelastic diffusion constant).

When the Cu^{2+} concentration equilibrates between the gel and the initially copper-free supernatant domain, the gel contracts to the height favored by the COOH groups [Fig. 1(c)]. As a control experiment, adding CuSO_4 into the

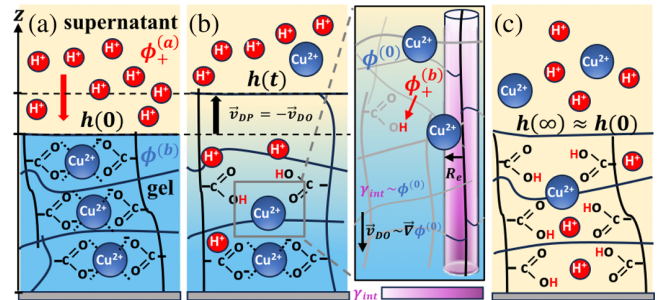


FIG. 1. PAA gel response to competing stimuli. (a) Acid (red, volume fraction $\phi_+^{(a)}$) is delivered from the supernatant solution into a copper-laden PAA hydrogel (on a substrate) with a contracted initial height $h(0) < H$ due to the chelation between COO^- and Cu^{2+} (blue, volume fraction $\phi^{(b)}$), which turns the gel blue. (b) The formation of COOH groups (volume fraction $\phi_+^{(b)}$) releases Cu^{2+} with a volume fraction $\phi^{(0)}$ into the gel solution. The gel swells with a time-dependent height $h(t) > h(0)$ and becomes colorless while a gradient $\nabla\phi^{(0)}$ along the $-z$ axis emerges [27]. The diffusiophoretic swelling velocity \mathbf{v}_{DP} negates the diffusio-osmotic solvent velocity \mathbf{v}_{DO} whose origin is shown in the inset: The steric repulsion between the polymers and copper ions at a core distance R_e yields a surface energy $\gamma_{\text{int}} R_e^2$ with a surface tension $\gamma_{\text{int}} \equiv k_B T \phi^{(0)} / 2k_f$, whose gradient ($\sim \nabla\phi^{(0)}$) sets the \mathbf{v}_{DO} direction. (c) The Cu^{2+} gradient, \mathbf{v}_{DO} , \mathbf{v}_{DP} eventually vanish due to Cu^{2+} diffusion, and the gel relaxes to the COOH-induced height $h(\infty) \approx h(0)$.

HCl solution suppressed the swelling, implying a reduction of the gel hypotonicity due to the temporary free copper gradient [27] (Sec. S1 in [34]). Understanding this single transient swelling and deswelling cycle may enable engineered gels that are bigger and still actuate much faster than current gel designs [50,51].

In this Letter, we address the following problem: Since osmosis is associated with interface selectivity to a solute, how does osmotic solvent influx into the gel emerge and diminish across the gel-supernatant interface that is fully permeable to the ions and acid? We hypothesize that this influx is “diffusio-osmotic” [Fig. 1(b)]: Steric repulsion between the proton-doped polymers and the free Cu^{2+} could lead to an interfacial tension $\gamma_{\text{int}} > 0$ proportional to the free ion volume fraction $\phi^{(0)}$ along the polymer-fluid interface. The solvent must then undergo Marangoni flow towards higher γ_{int} , known as diffusio-osmosis [52–54]. Momentum conservation demands that the diffusio-osmotic solvent velocity \mathbf{v}_{DO} be counteracted by the polymer displacement with a velocity $\mathbf{v}_{\text{DP}} = -\mathbf{v}_{\text{DO}}$ [Fig. 1(b)]. In analogy with colloidal and polymer diffusiophoresis [54,55], we define this reverse motion (i.e., poroelastic deformations) of the gel backbone as “gel diffusiophoresis.” To test this hypothesis, we develop a linear poroelastic theory for diffusiophoretic gel swelling caused by the released ion gradient [Fig. 1(b)]. Previously, hydrogels were used as solute beacons to enhance the diffusiophoretic colloid migration, albeit without coupling the gel mechanics and solute dynamics [56,57]. Moreover, although polyacrylate and polyacrylamide gels can transiently deform in response to osmolytes as heavy as 20–200 kDa, this was found to be due to the suppressed osmolyte diffusion in the gel [58–61]. Here we show how adding strong acid yields a diffusiophoretic swelling burst with a rate $\tau_{\text{total}}^{-1} > \tau^{-1}$ followed by gel contraction, in quantitative agreement with experiments. For weak acid, swelling is suppressed ($\tau_{\text{total}}^{-1} \lesssim \tau^{-1}$). Our theory confirms that molecules ($\lesssim 100$ Da) much smaller than typical osmolytes can induce diffusio-osmotic stress and deform the gel rapidly without impeding diffusion or interface selectivity.

We formulate the gel mechanics via a minimal Biot consolidation model [62–64]. Our model couples the gel mechanical response to the flow and concentration of the copper and acid as well as to the stresses they induce through association and dissociation with the gel backbone. In the gel domain, we use the incompressibility condition and the Darcy’s law for porous flow to determine the fluid velocity relative to the solid matrix \mathbf{v} and the solution pressure p (μ_f : kinematic viscosity) [34], i.e.,

$$\nabla \cdot \left(\mathbf{v} + \frac{\partial \mathbf{u}}{\partial t} \right) = 0, \quad \mathbf{v} = -\frac{k_f}{\mu_f} \nabla p. \quad (1)$$

The matrix displacement vector \mathbf{u} or equivalently the elastic strain tensor $\boldsymbol{\epsilon} \equiv [\nabla \mathbf{u} + (\nabla \mathbf{u})^T]/2$ is determined from the mechanical equilibrium condition for the gel stress tensor $\boldsymbol{\sigma}$

$$\nabla \cdot \boldsymbol{\sigma} = 0. \quad (2)$$

In $\boldsymbol{\sigma}$, the linear poroelastic terms comprise the elastic stresses (μ, λ : Lamé coefficients) and the solution pressure p . We add to these two contractility terms associated with the bound ions ($\tilde{\gamma}, \tilde{\chi}$: stress moduli), the osmotic pressure induced by the polymer volume fraction ϕ_p , and the diffusiophoretic term due to the interstitial free copper volume fraction $\phi^{(0)}$ (\mathbf{I} : rank-two identity tensor, k_B : Boltzmann’s constant, T : temperature, v_c : molecular volume) [34]:

$$\boldsymbol{\sigma} = 2\mu\boldsymbol{\epsilon} + \mathbf{I} \left[\lambda \text{Tr}(\boldsymbol{\epsilon}) - p + \tilde{\gamma}\phi^{(b)} + \tilde{\chi}\phi_+^{(b)} - \frac{k_B T}{v_c} \left(\eta_{\text{DP}}\phi^{(0)} + \frac{\phi_p^2}{2} \right) \right]. \quad (3)$$

The unitless diffusiophoretic coefficient satisfies $\eta_{\text{DP}} > 0$ ($\eta_{\text{DP}} < 0$) for repulsive (attractive) interactions between the polymer and the free copper. We consider steric repulsions with an exclusion radius R_e that leads to $\eta_{\text{DP}} \equiv R_e^2/2k_f > 0$, causing gel swelling when the free copper gradient is in the $-\hat{\mathbf{z}}$ direction [Fig. 1(b)] [34]. The interaction energy level of the steric repulsions $k_B T$ also constitutes a lower bound for the van der Waals interactions at distances comparable to R_e , whereas electrostatic effects are excluded since COOH groups are neutral (Sec. S1) [34]. From Eqs. (1), (3), the diffusiophoretic velocity is defined as $\mathbf{v}_{\text{DP}} \equiv -D_{\text{DP}}\nabla\phi^{(0)}$, where $D_{\text{DP}} \equiv k_B T R_e^2/2v_c\mu_f$ is the mobility [34,54]. We ignore a similar acid-gradient-driven effect since acid equilibrates across the two domains much faster than all timescales in this Letter. Because $D_{\text{DP}} \gg D$ holds, and the diffusiophoretic stress linear in $\phi^{(0)}$ can dominate the permanent polymeric osmotic stress quadratic in ϕ_p , controlled ionic release from the PAA gel can enable very high strain rates compared to mere osmotic absorption.

The internal gel stresses [Eq. (3)] are governed by the advection and diffusion of the free copper ($\phi^{(0)}$) and the free acid ($\phi_+^{(0)}$), as well as their conversion rates to/from the bound states $\phi^{(b)}$, $\phi_+^{(b)}$ on the gel backbone. They altogether satisfy $\phi_s + \phi_p + \phi^{(0)} + \phi_+^{(0)} + \phi^{(b)} + \phi_+^{(b)} = 1$ (ϕ_s : solvent volume fraction). Our model captures the evolution of $\phi^{(0)}$ and $\phi_+^{(0)}$ through the reaction-transport equations (D_x : diffusion constant of species x , \tilde{r} : rate constant, ϕ^* : COO^- volume fraction; Table S1 in [34])

$$\frac{\partial \phi^{(0)}}{\partial t} + \nabla \cdot \left[\overbrace{\phi^{(0)} \left(\mathbf{v} + \frac{\partial \mathbf{u}}{\partial t} \right) - D_{\text{Cu}} \nabla \phi^{(0)}}^{\equiv Q_{\text{Cu}}} \right] = \underbrace{\tilde{r}\phi_+^{(0)}\phi^{(b)} - \tilde{r}\phi^{(0)}\left[\phi^* - 2\phi^{(b)} - \phi_+^{(b)}\right]}_{\equiv R_{\text{Cu}}}, \quad (4)$$

$$\begin{aligned} \frac{\partial \phi_+^{(0)}}{\partial t} + \nabla \cdot \left[\overbrace{\phi_+^{(0)} \left(\mathbf{v} + \frac{\partial \mathbf{u}}{\partial t} \right) - D_+ \nabla \phi_+^{(0)}}^{\equiv \mathbf{Q}_+} \right] \\ = - \underbrace{\tilde{r} \phi_+^{(0)} (\phi^* - \phi_+^{(b)})}_{\equiv R_+}, \end{aligned} \quad (5)$$

where the flux terms \mathbf{Q}_{Cu} , \mathbf{Q}_+ involve particle advection and diffusion. The first term of the rate R_{Cu} describes the acid-induced Cu^{2+} release from the gel backbone, and the second term is the formation rate of a $\text{COO}^- - \text{Cu}^{2+} - \text{COO}^-$ chelate. The source term R_+ is the COOH formation rate. Then, $\phi^{(b)}$, $\phi_+^{(b)}$ are determined by the rate equations

$$\frac{\partial \phi^{(b)}}{\partial t} = -R_{\text{Cu}}, \quad \frac{\partial \phi_+^{(b)}}{\partial t} = R_+. \quad (6)$$

For simplicity, we assume a single rate constant \tilde{r} for all reactions in Eqs. (4)–(6) since they are experimentally found to be comparable (Sec. S2, Fig. S1 in [34]).

In the supernatant domain, denoting the fluid velocity by \mathbf{V} , the stress tensor by $\boldsymbol{\sigma}^{(a)}$, and the pressure by P , the incompressibility condition and the Stokes flow are

$$\nabla \cdot \mathbf{V} = 0, \quad \nabla \cdot \boldsymbol{\sigma}^{(a)} = 0; \quad \boldsymbol{\sigma}^{(a)} = \mu_f \nabla \mathbf{V} - \mathbf{I}P. \quad (7)$$

The copper ions with a volume fraction $\phi^{(a)}$ and acid with a volume fraction $\phi_+^{(a)}$ in the supernatant domain undergo only advection and diffusion with the fluxes $\mathbf{Q}_{\text{Cu}}^{(a)}$, $\mathbf{Q}_+^{(a)}$, governed by the mass conservation equations ($D_x^{(a)}$: diffusion constant of species x in the supernatant) [34]

$$\frac{\partial \phi^{(a)}}{\partial t} + \nabla \cdot \left[\overbrace{\phi^{(a)} \mathbf{V} - D_{\text{Cu}}^{(a)} \nabla \phi^{(a)}}^{\equiv \mathbf{Q}_{\text{Cu}}^{(a)}} \right] = 0, \quad (8)$$

$$\frac{\partial \phi_+^{(a)}}{\partial t} + \nabla \cdot \left[\overbrace{\phi_+^{(a)} \mathbf{V} - D_+^{(a)} \nabla \phi_+^{(a)}}^{\equiv \mathbf{Q}_+^{(a)}} \right] = 0. \quad (9)$$

Next, we determine the boundary conditions. The nonlinear differential equations (1)–(6) in the gel domain are coupled to Eqs. (7)–(9) in the supernatant domain through the following continuity conditions between the two domains ($\hat{\mathbf{n}}$: surface normal)

$$\begin{aligned} z = H: \mathbf{V} = \mathbf{v} + \frac{\partial \mathbf{u}}{\partial t}, \quad P - p = \frac{k_B T}{v_c} \left(\eta_{\text{DP}} \phi^{(0)} + \frac{\phi_p^2}{2} \right), \\ \hat{\mathbf{n}} \cdot \boldsymbol{\sigma} = \hat{\mathbf{n}} \cdot \boldsymbol{\sigma}^{(a)}, \quad \hat{\mathbf{n}} \cdot \mathbf{Q}_{\text{Cu}} = \hat{\mathbf{n}} \cdot \mathbf{Q}_{\text{Cu}}^{(a)}, \\ \hat{\mathbf{n}} \cdot \mathbf{Q}_+ = \hat{\mathbf{n}} \cdot \mathbf{Q}_+^{(a)}, \quad \phi^{(0)} = \phi^{(a)}, \quad \phi_+^{(0)} = \phi_+^{(a)}. \end{aligned} \quad (10)$$

The interfacial pressure jump $P - p$ is set by the polymer-induced osmotic stress that relaxes the gel to its equilibrium

state (without copper and acid), which we take as the reference state with zero strain. Adding a diffusio-osmotic agent (copper) will alter the gel solution pressure in the gel, which must equilibrate instantaneously across the interface [65,66], leading to the second condition in Eq. (10). The boundary conditions for the gel attached to a rigid, impermeable substrate at $z = 0$ and for the impermeable supernatant domain boundary at $z = H + H^{(a)}$ are given by ($H^{(a)}$: supernatant domain height) [34]

$$\begin{aligned} z = 0: \hat{\mathbf{n}} \cdot \mathbf{v} = 0, \quad \mathbf{u} = 0, \\ \hat{\mathbf{n}} \cdot \mathbf{Q}_{\text{Cu}} = 0, \quad \hat{\mathbf{n}} \cdot \mathbf{Q}_+ = 0, \end{aligned} \quad (11)$$

$$\begin{aligned} z = H + H^{(a)}: \mathbf{V} = 0, \quad P = 0, \\ \hat{\mathbf{n}} \cdot \mathbf{Q}_{\text{Cu}}^{(a)} = 0, \quad \hat{\mathbf{n}} \cdot \mathbf{Q}_+^{(a)} = 0. \end{aligned} \quad (12)$$

To explain the vertical deformation dynamics in Ref. [27], we consider first, 1D uniaxial deformations in response to a uniform acid front advancing in the $-\hat{\mathbf{z}}$ direction to the copper-laden gel and, second, 2D deformations due to an acid front with a Gaussian weak perturbation to investigate the effect of the potential nonuniformities during acid delivery in the experiments. In the linear elastic limit, we take the polymer volume fraction ϕ_p and the COOH volume fraction ϕ^* constant by ignoring the effect of small deformations on the concentrations [34]. In one dimension, we denote the magnitudes of all vectors by $u_z(z, t) \equiv |\mathbf{u}|$, $v(z, t) \equiv |\mathbf{v}|$, $V(z, t) \equiv |\mathbf{V}|$. All nonvanishing tensors reduce to a scalar, i.e., $\sigma_{zz} \equiv \hat{\mathbf{z}} \cdot \boldsymbol{\sigma} \cdot \hat{\mathbf{z}}$, $\epsilon_{zz} \equiv \hat{\mathbf{z}} \cdot \boldsymbol{\epsilon} \cdot \hat{\mathbf{z}} = \partial u_z / \partial z$, $\hat{\mathbf{z}} \cdot \mathbf{I} \cdot \hat{\mathbf{z}} = 1$. Eqs. (1)–(12) determine the uniaxial deformations as follows: Per Eqs. (10)–(12), the incompressibility conditions in Eqs. (1), (7) reduce to $v + \partial u_z / \partial t = 0$ and $V = 0$, i.e., local gel deformations do not impose any net flow in the lab frame. This also leads to a diffusive stimulus dynamics in Eqs. (4), (5), (8), and (9). Then, using the unitless variables $u'_z \equiv u_z / H$, $z' \equiv z / H$ (gel), $z' \equiv z / H^{(a)}$ (supernatant), $t' \equiv t / \tau$ where $\tau \equiv \mu_f H^2 / k_f \bar{p}$, $\bar{p} \equiv (2\mu + \lambda)$, and dropping their primes, Eqs. (1)–(3) yield a dimensionless evolution equation for the gel displacement as ($\gamma \equiv \tilde{\gamma} / \bar{p}$, $\chi \equiv \tilde{\chi} / \bar{p}$, $\nu_{\text{DP}} \equiv k_B T \eta_{\text{DP}} / v_c \bar{p}$) [34]

$$\frac{\partial u_z}{\partial t} = \frac{\partial^2 u_z}{\partial z^2} + \gamma \frac{\partial \phi^{(b)}}{\partial z} + \chi \frac{\partial \phi_+^{(b)}}{\partial z} - \nu_{\text{DP}} \frac{\partial \phi^{(0)}}{\partial z} \quad (13)$$

with the boundary conditions from Eqs. (10), (11) ($\hat{\mathbf{n}} = \hat{\mathbf{z}}$)

$$u_z|_{z=0} = 0, \quad \left. \frac{\partial u_z}{\partial z} \right|_{z=1} = -\gamma \phi^{(b)} - \chi \phi_+^{(b)}. \quad (14)$$

Equations (13), (14) are closed by the unitless forms of Eqs. (4)–(6), (8), (9) [i.e., Eqs. (S10)–(S14); Sec. S2 [34]] and the corresponding boundary conditions in Eqs. (10)–(12)

with the unitless parameters in Table S1 [34]. The seven initial conditions for the contracted gel with stored Cu^{2+} are

$$u_z = -\gamma\phi^{(b)}z, \quad \phi^{(b)} = \frac{\phi^*}{2}, \quad \phi_+^{(b)} = \phi^{(0)} = \phi_+^{(0)} = 0, \quad (15a)$$

and in the supernatant solution

$$\phi^{(a)} = 0, \quad \phi_+^{(a)}(z) = \frac{\phi_{+,i}^{(a)}}{2} [1 + \tanh(\Gamma(z - z_0))], \quad (15b)$$

where $\Gamma = \Gamma^{(1D)}$ and $z_0 = z_0^{(1D)}$ [34].

Our main results are demonstrated in Fig. 2. The simulation procedure and postprocessing of the experimental data are detailed in Sec. S3, and the validity of the linear poroelastic model is discussed in Sec. S4 [34]. Upon the diffusion of 1 M acid ($\phi_{+,i}^{(a)} = 0.006$) into the copper-laden gel from the supernatant domain, the gel height exhibits a temporal spike with a magnitude $\lesssim 0.1H$ in quantitative agreement with experiments [Fig. 2(a)]. This rapid swelling followed by the slower contraction can be understood by considering the interplay among the acid flux and its complexation, the subsequent release of bound copper and the diffusiphoretic swelling induced by it, and the gel relaxation at longer times [Figs. (S2)–(S4)] [34]: Although our theory suggests that diffusiphoresis can induce rapid gel deformations at a timescale $\tau/\nu_{DP} \ll \tau$, the swelling rate is limited by the overall release time $\tau_{\text{total}} \approx 0.82\tau$ of the height-averaged bound copper $\phi_{\text{total}}^{(b)}$ [Fig. 2(b)]. As a result, the gel undergoes continual diffusiphoretic swelling until $t \approx \tau_{\text{total}}$ when the height reaches maximum [Fig. 2(a)]. This short swelling time $\tau_{\text{total}} < \tau$ can further be improved by considering nonlinear deformations driven by higher acid concentrations. The decay from the maximum height is governed by the competition between the diffusive relaxation of the deformations and the residual diffusiphoretic swelling. This leads to a subdiffusive relaxation with a timescale $\tau_{r,1} \approx 0.54\tau$, which is higher than the timescale $\tau_D \equiv 4\tau/\pi^2 \approx 0.4\tau$ of the purely diffusive relaxation dynamics (Sec. S5, Fig. S5, S6) [34]. Diffusion ceases at $t \gtrsim 4\tau$, and the longtime slow relaxation is governed by the ever damping diffusiphoretic term with a timescale $\tau_{r,2} \approx 5.2\tau$ [34]. A similar swelling was also observed upon 1M acid entry to a softer hydrogel that initially stores Ca^{2+} [27]. In our simulations, when the initial acid front is brought closer to the gel-supernatant interface and the unitless stress moduli χ, γ are fitted accordingly for a calcium-laden softer gel, our results agree well with the experiments (Sec. S6, Fig. S7 [34]).

To validate that the swelling in Fig. 2(a) is driven by the rapid Cu^{2+} release in the experiments, the same acid amount was slowly added over successive steps with concentrations ranging from 0.01M to 1M, which lead

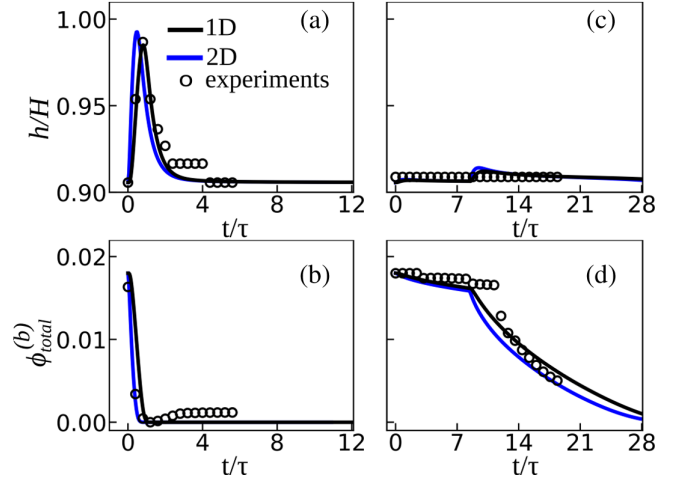


FIG. 2. Gel deformations upon acid addition. The gel height $h/H \equiv 1 + u_z$ versus time for (a) $\phi_{+,i}^{(a)} = 0.006$ (equivalent to $\sim 1M$ acid) and (c) the stepwise addition of acid with $\phi_{+,i}^{(a)} = 6 \times 10^{-5}$ ($\sim 0.01M$) initially and $\phi_{+,i}^{(a)} = 3 \times 10^{-4}$ ($\sim 0.05M$) at $t/\tau = 8.4$, respectively [see Eq. (15b)]. (b),(d) Time dependence of the total bound copper $\phi_{\text{total}}^{(b)} \equiv \int_0^1 \phi^{(b)} dz$ corresponding, respectively, to (a) and (c). The 2D h/H and $\phi_{\text{total}}^{(b)}$ profiles show the average values over the experimental distance between two adjacent microplates ($= 5 \mu\text{m}$) about the horizontal center of the gel film ($x/L = 0.5 \pm 1 \times 10^{-4}$).

to no deformation [Fig. 2(c), circles] [27]. Here we simulate only the first two steps with $\phi_{+,i}^{(a)} = 6 \times 10^{-5}$ ($\sim 0.01M$) at $t = 0$ and $\phi_{+,i}^{(a)} = 3 \times 10^{-4}$ ($\sim 0.05M$) at $t = 8.4\tau$. Our numerical results yield marginal deformations about $0.1\%H$ and $0.5\%H$ that fall within the experimental error of $\pm 1\%H$ [Fig. 2(c)]. Swelling is suppressed for the low acid concentrations since the bound Cu^{2+} release rate is drastically reduced [Fig. 2(d)]. In this limit, the gel poroelastic relaxation balances the diffusiphoretic swelling that is slowed down by the low bound copper release rate.

Although the 2D weakly perturbed gel swelling and bound copper release profiles deviate only slightly from the 1D uniaxial deformation results [Figs. 2(a)–2(d)], the 2D simulations reveal the swelling and relaxation dynamics starting from the initial conditions (Sec. S3) [34]. When adding 1M acid initially [Fig. 3(a)], the penetration of the Gaussian stimulus front (with a standard deviation in the order of the water capillary length) into the gel triggers a local swelling bump associated with a convective flow [Figs. 3(b)–3(c), movie S1 in [34]]. The flow reverses direction at the center ($x = L/2$) at the onset of breakup of the single bump into two swelling fronts [$t = 0.5\tau$, Fig. 3(d)], which travel in opposite directions at the gel surface in phase with the copper decomplexation front [$t = 0.7\tau$, Fig. 3(e)] and decay at longer times along with the diminishing flow streamlines. Similar traveling

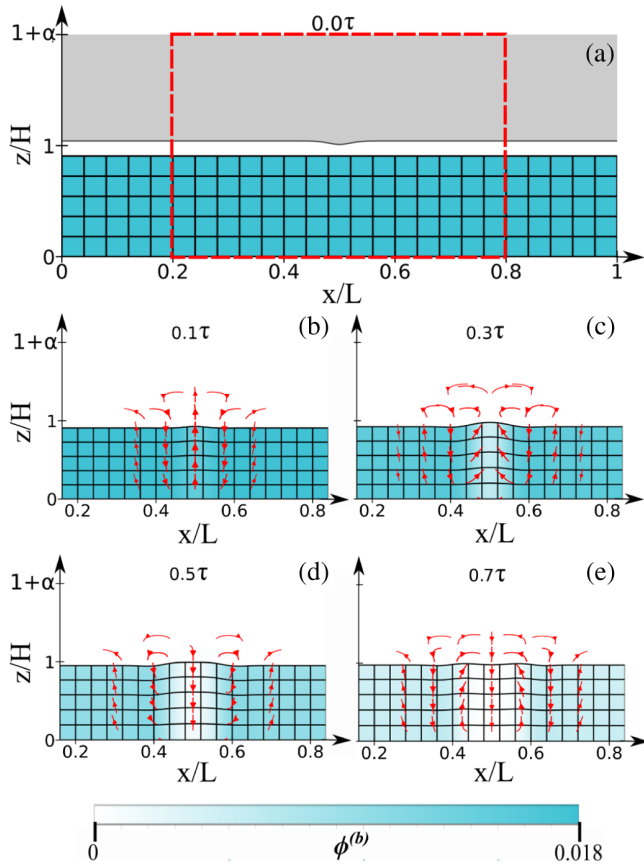


FIG. 3. 2D gel response to 1M acid. (a) For 1M acid with a Gaussian perturbation [Eqs. (15b),(S15)], the dynamics at (b) $t = 0.1\tau$, (c) $t = 0.3\tau$, (d) $t = 0.5\tau$, and (e) $t = 0.7\tau$ within the boxed region ($\alpha = 770$). The red streamlines indicate the computed fluid flow in the lab frame (line width: logarithm of the flow speed, arrows: flow direction).

deformation fronts sensitive to the acid progression rate and direction were reported in Ref. [27]. For 0.05M acid delivery at $t = 8.4\tau$ after the initial 0.01M acid addition step, because the deformation and flow are negligible, a traveling front at the gel surface does not form (Fig. S8, Movie S2) [34].

Our theory explains the fast swelling of the PAA gel by introducing a gel diffusiophoresis mechanism, which nevertheless needs to be validated by microscopic approaches such as molecular dynamics simulations. Furthermore, the linear poroelastic swelling in Fig. 2(a) only produces a strain rate of $\sim 0.04 \text{ s}^{-1}$ and a power density of $\sim 11.1 \text{ mW/kg}$ (Sec. S7, Fig. S9 [34]), which are surpassed by certain gels that generate 0.2 s^{-1} and 260 mW/kg and PAA microgel suspensions that swell from the dry state and achieve 230 mW/kg [24,26,34]. Therefore, our analysis must be extended to nonlinear large deformations to test high strain rates and power densities based on $D_{DP} \gg D$ allowed by the gel diffusiophoresis [65,67]. This inequality can also be engineered in other gels to scale up chemically responsive shape-shifting hydrogel actuators. Also, hydrogels that

combine diffusiophoresis with periodic actuations via cyclic chemical feedback (as those in Belousov-Zhabotinsky gels [25,68]) must be designed for engineering applications. These steps will pave the way for internally powered gel-based proof-of-concept soft robots with enhanced precision, versatility, and dexterity.

We thank J. Aizenberg, J. Barone, S. Cheng, J. Gray, A. Grinthal, M. Pleimling, and W. Shu for fruitful discussions and the Virginia Tech College of Science for financial support. We acknowledge the Virginia Tech Advanced Research Computing Center for computing resources.

*nadirkaplan@vt.edu

- [1] T. Kanahama, S. Tsugawa, and M. Sato, *Sci. Rep.* **13**, 2063 (2023).
- [2] K. Schulgasser and A. Witztum, *Ann. Bot.* **80**, 35 (1997).
- [3] C. W. Gottschalk, *Am. J. Med.* **36**, 670 (1964).
- [4] J. L. Stephenson, *Kidney Int.* **2**, 85 (1972).
- [5] D. Brogioli, *Phys. Rev. Lett.* **103**, 058501 (2009).
- [6] R. A. Tufa, S. Pawlowski, J. Veerman, K. Bouzek, E. Fontananova, G. di Profio, S. Velizarov, J. Goulo Crespo, K. Nijmeijer, and E. Curcio, *Appl. Energy* **225**, 290 (2018).
- [7] G. M. Geise, H. B. Park, A. C. Sagle, B. D. Freeman, and J. E. McGrath, *J. Membr. Sci.* **369**, 130 (2011).
- [8] J. R. Werber, C. O. Osuji, and M. Elimelech, *Nat. Rev. Mater.* **1**, 16018 (2016).
- [9] B. E. Logan and M. Elimelech, *Nature (London)* **488**, 313 (2012).
- [10] A. Siria, P. Poncharal, A.-L. Biance, R. Fulcrand, X. Blase, S. T. Purcell, and L. Bocquet, *Nature (London)* **494**, 455 (2013).
- [11] A. Siria, M.-L. Bocquet, and L. Bocquet, *Nat. Rev. Chem.* **1**, 0091 (2017).
- [12] O. Kedem and A. Katchalsky, *J. Gen. Physiol.* **45**, 143 (1961).
- [13] Y. S. Zhang and A. Khademhosseini, *Science* **356** (2017).
- [14] R. V. Uljin, N. Bibi, V. Jayawarna, P. D. Thornton, S. J. Todd, R. J. Mart, A. M. Smith, and J. E. Gough, *Materials Today* **10**, 40 (2007).
- [15] T. S. Shim, S.-H. Kim, C.-J. Heo, H. C. Jeon, and S.-M. Yang, *Angew. Chem.* **124**, 1449 (2012).
- [16] A. Bordbar-Khiabani and M. Gasik, *Int. J. Mol. Sci.* **23**, 3665 (2022).
- [17] H. Yuk, S. Lin, C. Ma, M. Takaffoli, N. X. Fang, and X. Zhao, *Nat. Commun.* **8**, 14230 (2017).
- [18] M. Ma, L. Guo, D. G. Anderson, and R. Langer, *Science* **339**, 182 (2013).
- [19] L. Dong, A. K. Agarwal, D. J. Beebe, and H. Jiang, *Nature (London)* **442**, 551 (2006).
- [20] G. Zabow, S. J. Dodd, and A. P. Koretsky, *Nature (London)* **520**, 73 (2015).
- [21] M. Skoge, H. Yue, M. Erickstad, A. Bae, H. Levine, A. Groisman, W. F. Loomis, and W.-J. Rappel, *Proc. Natl. Acad. Sci. U.S.A.* **111**, 14448 (2014).
- [22] J. M. Nerbonne and R. S. Kass, *Phys. Rev.* **85**, 1205 (2005).

- [23] M. Péter, A. Glatz, P. Gudmann, I. Gombos, Z. Török, I. Horváth, L. Vögh, and G. Balogh, *PLoS One* **12**, e0173739 (2017).
- [24] H. Choudhary and S.R. Raghavan, *ACS Appl. Mater. Interfaces* **14**, 13733 (2022).
- [25] Y. Zhang, N. Zhou, N. Li, M. Sun, D. Kim, S. Fraden, I. R. Epstein, and B. Xu, *J. Am. Chem. Soc.* **136**, 7341 (2014).
- [26] L. Arens, F. Weißenfeld, C. O. Klein, K. Schlag, and M. Wilhelm, *Adv. Sci.* **4**, 1700112 (2017).
- [27] P. A. Korevaar, C. N. Kaplan, A. Grinthal, R. M. Rust, and J. Aizenberg, *Nat. Commun.* **11**, 386 (2020).
- [28] F. Velazquez, S. Y. Peak-Chew, I. S. Fernández, C. S. Neumann, and R. R. Kay, *Chem. Biol.* **18**, 1252 (2011).
- [29] L. Mahadevan and P. Matsudaira, *Science* **288**, 95 (2000).
- [30] E. Palteau, D. Morales, M. D. Dickey, and O. D. Velev, *Nat. Commun.* **4**, 2257 (2013).
- [31] G. S. Longo, M. Olvera de la Cruz, and I. Szleifer, *J. Chem. Phys.* **141**, 124909 (2014).
- [32] G. S. Longo, M. Olvera de la Cruz, and I. Szleifer, *Soft Matter* **12**, 8359 (2016).
- [33] A. Drozdov, C.-G. Sanporean, and J. deClaville Christiansen, *Mater. Today Commun.* **6**, 92 (2016).
- [34] See Supplemental Material at <http://link.aps.org/supplemental/10.1103/PhysRevLett.132.208201>, which includes Refs. [35–49], for the supporting text, table for the physical and simulation parameters, figures, and movies.
- [35] See the repository at [10.5281/zenodo.10944564](https://doi.org/10.5281/zenodo.10944564) for computational codes and movies S1 and S2.
- [36] P. J. Flory and J. J. Rehner, *J. Chem. Phys.* **11**, 521 (1943).
- [37] J. N. Israelachvili, in *Intermolecular and Surface Forces (Third Edition)*, edited by J. N. Israelachvili (Academic Press, San Diego, 2011), pp. 107–132.
- [38] J. N. Israelachvili, in *Intermolecular and Surface Forces (Third Edition)*, edited by J. N. Israelachvili (Academic Press, San Diego, 2011), pp. 253–289.
- [39] M. S. Alnaes, J. Blechta, J. Hake, A. Johansson, B. Kehlet, A. Logg, C. Richardson, J. Ring, M. E. Rognes, and G. N. Wells, *Arch. Numer. Software* **3** (2015).[10.11588/ans.2015.100.20553](https://doi.org/10.11588/ans.2015.100.20553)
- [40] COMSOL AB, Stockholm, Sweden, COMSOL Multiphysics® 5.4, www.comsol.com (2018).
- [41] D. Tzeli, G. Theodorakopoulos, I. D. Petsalakis, D. Ajami, and J. Rebek, *J. Am. Chem. Soc.* **133**, 16977 (2011).
- [42] J. Alí-Torres, J.-D. Maréchal, L. Rodríguez-Santiago, and M. Sodupe, *J. Am. Chem. Soc.* **133**, 15008 (2011).
- [43] B. A. Baker, R. L. Murff, and V. T. Milam, *Polymer* **51**, 2207 (2010).
- [44] R. Sunyer, A. J. Jin, R. Nossal, and D. L. Sackett, *PLoS One* **7**, 1 (2012).
- [45] A. K. Denisin and B. L. Pruitt, *ACS Appl. Mater. Interfaces* **8**, 21893 (2016).
- [46] M. A. Hossain, C. K. Roy, S. D. Sarker, H. Roy, A. H. Howlader, and S. H. Firoz, *Mater. Adv.* **1**, 2107 (2020).
- [47] C. Knight and G. A. Voth, *Acc. Chem. Res.* **45**, 101 (2012).
- [48] N. Agmon, *Chem. Phys. Lett.* **244**, 456 (1995).
- [49] Z. C. Wu, Y. Awakura, S. Ando, and H. Majima, *Mater. Trans., JIM* **31**, 1065 (1990).
- [50] Z. Zhang, Z. Chen, Y. Wang, J. Chi, Y. Wang, and Y. Zhao, *Small Methods* **3**, 1900519 (2019).
- [51] Y. Zhang, P. Li, K. Zhang, and X. Wang, *Langmuir* **38**, 15433 (2022).
- [52] B. Derjaguin, G. Sidorenkov, E. Zubashchenko, and E. Kiseleva, *Prog. Surf. Sci.* **43**, 138 (1993).
- [53] C. Lee, C. Cottin-Bizonne, A.-L. Biance, P. Joseph, L. Bocquet, and C. Ybert, *Phys. Rev. Lett.* **112**, 244501 (2014).
- [54] S. Marbach and L. Bocquet, *Chem. Soc. Rev.* **48**, 3102 (2019).
- [55] S. Ramírez-Hinestrosa, H. Yoshida, L. Bocquet, and D. Frenkel, *J. Chem. Phys.* **152**, 164901 (2020).
- [56] A. Banerjee, I. Williams, R. N. Azevedo, M. E. Helgeson, and T. M. Squires, *Proc. Natl. Acad. Sci. U.S.A.* **113**, 8612 (2016).
- [57] A. Banerjee, H. Tan, and T. M. Squires, *Phys. Rev. Fluids* **5**, 073701 (2020).
- [58] J. J. F. Sleebom, P. Voudouris, M. T. J. J. M. Punter, F. J. Aangenendt, D. Florea, P. van der Schoot, and H. M. Wyss, *Phys. Rev. Lett.* **119**, 098001 (2017).
- [59] F. J. Aangenendt, M. T. J. J. M. Punter, B. M. Mulder, P. van der Schoot, and H. M. Wyss, *Phys. Rev. E* **102**, 062606 (2020).
- [60] M. T. J. J. M. Punter, H. M. Wyss, and B. M. Mulder, *Phys. Rev. E* **102**, 062607 (2020).
- [61] J. Tong and J. Anderson, *Biophys. J.* **70**, 1505 (1996).
- [62] J. R. Sachs, M. R. Glucksberg, O. E. Jensen, and J. B. Grotberg, *J. Appl. Mech.* **61**, 726 (1994).
- [63] M. A. Biot, *J. Appl. Phys.* **12**, 155 (1941).
- [64] M. Doi, *J. Phys. Soc. Jpn.* **78**, 052001 (2009).
- [65] W. Hong, X. Zhao, J. Zhou, and Z. Suo, *J. Mech. Phys. Solids* **56**, 1779 (2008).
- [66] W. Hong, Z. Liu, and Z. Suo, *Int. J. Solids Struct.* **46**, 3282 (2009).
- [67] C. W. MacMinn, E. R. Dufresne, and J. S. Wettlaufer, *Phys. Rev. Appl.* **5**, 044020 (2016).
- [68] P. Dayal, O. Kuksenok, and A. C. Balazs, *Proc. Natl. Acad. Sci. U.S.A.* **110**, 431 (2013).